Materials and Methods

Protein Purification. Full length arrestin-3 and its truncated form (residues 1-393), ASK1, GST-MKK4-His_6, GST-MKK7-His_6, JNK3-His_6, and MBP-fusion proteins were purified, as described previously (1-5). In brief, MKK4 and MKK7 were cloned into a pGEX-4T1 vector with an N-terminal cleavable GST-tag and a C-terminal cleavable His-tag. To generate activated MKK4 and MKK7, 4 μM GST-MKK4 or GST-MKK7 and 2 μM GST-MEKK1c (catalytic domain) were incubated at 30°C for 1 h in the presence of 4 mM ATP in 10 mL activation buffer (25 mM HEPES pH 7.5, 20 mM $MgCl_2$, 0.1 mM EDTA, 0.1 mM EGTA, 2 mM dithiothreitol). Proteins were re-purified via size exclusion chromatography on a Superdex S200 Increase 10/300 GL column equilibrated with 25 mM HEPES-Na, pH 7.5, 100 mM KCl, 0.1 mM EDTA, 0.1 mM EGTA and 2 mM TCEP to separate activated GST-MKK4/7 from constitutively active GST-MEKK1c. JNK3-His was cloned into the pTrc-His2 vector with a C-terminal His-tag. Active JNK3 was prepared in the presence of active MAP2Ks, 4mM ATP, 20 mM $MgCl_2$, 0.1 mM EDTA, 0.1 mM EGTA, and 2 mM dithiothreitol.

Microscale Thermophoresis. MST was performed using the Monolith NT.115 instrument (NanoTemper Technologies GmbH). Binding was measured between arrestin-3 (in 20 mM MOPS pH 7.5, 150 mM NaCl, and 2 mM TCEP) and a His-tagged kinase. The His-tagged proteins were labeled using the MO-L008 Monolith™ His-Tag Labeling Kit RED-tris-NTA following the manufacturer's protocol (100 nM final concentration of kinase in PBS-T buffer). This labeling dye has recently been described as the optimal conjugate for oligohistidine-tags (6). An experiment with a control His peptide was performed to demonstrate that the His-tag did not interfere with binding. A 16-step dilution series was prepared by adding 10 μL buffer (20 mM MOPS pH 7.5, 150 mM NaCl, 2 mM TCEP, 0.05% Tween-20) to 15 tubes. 20 μL of 43-110 μM arrestin-$3^{(1-393)}$ was placed in the first tube, and 10 μL was transferred to the second tube and mixed well by pipetting (1:1 dilution series). The final tube did not contain any arrestin-3 and was used as a blank. 10 μL of the binding partner (inactive or phosphorylated His-kinase in the presence of 1 mM ATP and 2 mM $MgCl_2$) was added to each tube of the dilution series (final concentration 50 nM). The samples were incubated on ice for 15 minutes before being transferred to Standard Monolith NT™ Capillaries. The capillaries were scanned using the MST instrument (40% LED, 40% MST power). The preliminary capillary scan did not show a significant difference in the amount of fluorescently labeled His-kinase during experimentation except for several high concentrations of arrestin-3 (marked in **Fig. S2**). An SDS-denaturation test was performed, and it was determined that at high concentrations of arrestin-3, several samples exhibited ligand dependent fluorescent changes. These data was excluded from further analysis. All data were analyzed using PALMIST (7, 8). Measured fluorescence was normalized and averaged, and the binding constants were determined using a global fit calculation and a 1:1 fitting model (except for the IP_6 model where a 1:2 macro fit was chosen). The preset Thermophoresis + T-jump was used to calculate binding isotherms for the MAP2Ks, while the preset T-jump was used for the JNK3 interactions. Inactive and active kinase forms were compared using either a Student's two-tailed t-test (MAP2Ks: MKK4 and MKK7) or One-way ANOVA followed by Dunnet's post-hoc test (JNK3) using the inactive kinase form as the control. Of note, for **Fig. 1B** and **Fig 1H** we were only able to obtain the lower boundary K_d values. To perform the Student's t-test we assumed that the values obtained from the lower boundary followed a normal distribution, which allowed us to determine significant difference.

MBP Pull-down. N-terminal MBP-fusion proteins including full-length bovine arrestin-3 and sequences corresponding to the indicated arrestin elements were designed and purified, as previously described (9, 10). In brief, arrestin-3 or arrestin-3 fragments were subcloned into a pMal-p2T vector with a 10 amino acid linker, TLVPRGSPGF, between MBP and arrestin-3 or its fragments. Purified MBP was used as a negative control in all pull-down experiments and non-specific binding was subtracted from the total observed binding for each construct. MBP-fusion proteins (10-30 μg in 50 μL of 20 mM Tris/150 mM NaCl) were immobilized on amylose resin (25 μL, 50% slurry, New England Biolabs) for 1 h at 4 °C with slight rotation. Prey protein (GST-MKK4, GST-MKK7, or His-JNK3, 10 μg in 50 μL of 20 mM Tris/150 mM NaCl) was added to the immobilized MBP constructs and incubated with gentle rotation for 2 h at 4 °C in the presence or absence of 2 mM ATP and 4 mM $MgCl_2$. Samples were transferred to centrifuge filters (Durapore®-PVDF-0.65 μm), washed three times with 50 mM HEPES-Na, pH 7.3, 150 mM NaCl. Elution buffer (100 μL 50 mM maltose in wash buffer) was added, the samples were rotated gently for 5 min at 4 °C before centrifugation. Protein in eluates was precipitated by the addition of 1 mL of methanol, and centrifugation at

maximum speed for 10 min. The pellets were air dried, dissolved in SDS sample buffer (30 µL Laemmli, 2x) and analyzed by SDS-PAGE and Western blotting, as described (9). Statistical analysis was performed using One-way ANOVA followed by Dunnett's post-hoc test.

Peptide Array Synthesis. The ResPep SL peptide synthesizer was used with conventional SPOT synthesis protocols using peptides ranging from 14 to 25 residues in length, as previously described (11). Both a blank spot and a 15-mer glycine peptide were used as negative controls, and non-specific binding to these controls was not statistically different. Peptides were assembled by the ResPep SL on solid support via a peptide amide linker using Fmoc-chemistry. The sequences of the peptides were derived from the first 25 amino acids of bovine arrestin-3, which function as an effective scaffold of ASK1-MKK4/7-JNK3 cascade in cells (10). After synthesis, the amino-protecting group was removed using piperidine (20% (v/v) solution in dimethylformamide) followed by extensive washing. The membranes were then submerged in a solution of 95% trifluoroacetic acid (TFA) and 3% triisopropylsilane for 1 h with agitation. Following removal of the TFA solution, the membranes were washed in dichloromethane four times 10 min each, followed by four 10 min washes in dimethylformamide and two 2 min washes in ethanol. The membranes were then dried in the hood and stored at 4°C.

Peptide Membrane Blots. Dried membranes were soaked in 100% ethanol for 5 min and then rehydrated by washing twice in water for 5 min. The membranes were then incubated in blocking solution (5% non-fat dry milk in Tris-buffered saline (TBS) with 0.1% Tween 20) for 1 h. The membranes were washed five times for 5 min before overnight incubation at 4°C with the prey protein (0.3-0.5 µM, depending on the protein construct) in binding buffer, (20 mM HEPES pH 7.3, 50 mM KCl, 0.1 mM EDTA, 0.1 mM EGTA, 10% glycerol, 2 mM ATP, 4 mM $MgCl_2$). The following morning, the membranes were rinsed five times for 5 min in TBS with 0.1% Tween 20. Membranes were incubated with the appropriate primary antibody for 1 h at room temperature, washed five times for 5 min in TBS with 0.1% Tween 20 (SAPK/JNK Rabbit Cell Signaling, 1:1,000 dilution, #9252P; GST Rabbit Cell Signaling, 1:1,000 dilution, #2622; ASK1 Rabbit Cell Signaling, 1:1,000 dilution, #3762). The corresponding HRP-conjugated secondary antibody (1:10,000 dilution) was prepared in TBS with 0.1% Tween 20, incubated with the membrane for 1 h, followed by two 5 min washes in TBS at room temperature. The spots were visualized using the SuperSignal West Pico Stable Peroxide Solution kit from ThermoScientific. Images were obtained using the Bio-Rad Gel Doc Imager and analyzed by densitometry using ImageJ protein array analyzer. For ResPep analysis, the signal in individual dots was measured as a percentage of total binding density detected on the membrane. This allowed for comparison across all peptide experiments. Statistical analysis was performed using one-way ANOVA followed by Dunnett's post-hoc test using GraphPad Prism5.

Computational Modeling. The JNK3 activation reaction model (JARMv1.0) was implemented in Python using the PySB framework (12) that allows users to build mathematical models of biochemical systems as Python programs. In all, JARMv1.0 included 28 biochemical species, 60 chemical reactions, and 44 free parameters. When this program is executed, a set of rules is translated to 28 ordinary differential equations (ODEs) using the mass action kinetics formalism. Since the ODEs generated by JARM require rate constants instead of K_D values, all experimental K_D were converted into rate parameters using the equation $K_D=k_r/k_f$. For the model calibration, k_f rates were set within the "average enzyme" distribution of specificity constants (13-15), whereas the k_r were allowed to change. Out of linear range values at initial time points and higher than theoretical maximum values in the time-course data (Fig. 2A) were set to zero and the theoretical maximum, respectively. We then applied scaling normalization to both the time-course data and the simulated trajectories. Model calibration was then performed using the PyDREAM package (16), which is a python implementation of the (Multiple-Try) Differential Evolution Adaptive Metropolis ($DREAM_{(ZS)}$) algorithm (17). To reduce the number of model parameters to calibrate, we used the experimentally measured dissociation constants for the interactions between MKK4/7, JNK3, and arrestin-3, and literature values for the interactions between MKK4/7 and JNK3 alone (18). We assumed that the catalytic constants for JNK3 phosphorylation were the same within a scaffold complex and in solution (supported by **SI Appendix, SFig. 6**). The model was pre-equilibrated to allow complexes to form before the reaction is initiated. Parameter prior probabilities were specified as uniform distributions with the lower and upper boundary set with the lowest and highest values from the protein–protein kinetic interaction data and structures (PPKIDS) dataset (19), indicating a lack of knowledge about the likely parameter values. Literature-based values and experimental measures were fixed. The fit of simulated trajectories to experimental data was measured using the sum of the squared differences:

$$\chi^2 = \sum_t \sum_i \frac{1}{2\sigma^2_{data}} [x^i_{model}(t;\Theta) - x^i_{data}(t)]^2$$

Where *t* is the time span of the simulation and experiments, $\Theta = (\theta_1, \ldots, \theta_n)$ are the parameters of the model, x^i_{model} are the simulations of the model under condition *i and* x^i_{data} (t) is the experimental data under condition *i*. This function corresponds to the negative log of the likelihood in the Bayesian framework assuming the measurement errors at time *t* have a normal distribution. By minimizing this function, we find probable parameter sets that fit the experimental data within the constraints that the network interactions and the network kinetics imposes. To further constraint the model, we added the requirement that thermodynamic cycles present in the interaction network (**SI Appendix, Fig. S5A**) must obey detailed balance/free energy conservation in the likelihood function.

The DREAM$_{(ZS)}$ algorithm was ran using PyDREAM with five chains that started in parameter locations provided by previous calibrations using the Particle Swarm Optimization algorithm (20). Each chain sampled 500,000 parameter sets and the first 250,000 samples were discarded as burn-in. All chains were tested for convergence using the Gelman-Rubin criterion. To measure the goodness of fit of the calibrated model to the experimental data we use the χ^2 statistic. A good fit would correspond to a χ^2 value that is approximately equal to the number of experimentally obtained data points. Using the 5000 most likely parameters obtained from the calibration we obtained a χ^2 value of 32.32 (±0.09). Given that we measured 36 experimental points for pTyr-JNK3 and pThr-JNK3 reactions, we conclude that the model shows a reasonable fit to the experimental data.

All code used to build the model, fit the model parameters and perform analysis is freely distributed as open-source software and available in the Lopez lab GitHub repository (github.com/LoLab-VU/JARM).

In vitro kinase activation assay. The ability of purified active MKK4 and MKK7 to phosphorylate inactive JNK3 in the presence of arrestin-3 was tested using an in vitro activation assay. A stock tube of kinase mix (10 mM HEPES pH 7.3, 5 mM $MgCl_2$, 100 mM NaCl, 2 mM TCEP) was prepared with pMKK4 (0.05 µM), pMKK7 (0.05 µM), arrestin-3$^{(1\text{-}393)}$ (5 µM), and inactive JNK3 (0.5 µM). Each reaction was performed in a volume of 20 µL in a 30°C water bath for the indicated time (0-180 secs). Reactions were initiated by adding 2 µL 10 mM ATP (1 mM final concentration) and quenched with 20 µL SDS buffer. Western analysis using pTyr (Cell Signaling, 1:2000 dilution, #8954S) or pThr (Cell Signaling, 1:5000 dilution, #9391S) antibodies was used to assess JNK3 phosphorylation. Known concentrations of ppJNK3 (20 – 340 ng) were used as standards in all experiments. Bands were quantified using Quantity One software (Bio-Rad) and phospho-JNK3 (ng) was plotted as a function of time (sec).

Recombinant pcDNA3-arrestin-3-JNK3 construction. To make the arrestin-3-JNK3 fusion the cDNAs encoding full-length arrestin-3 and full-length JNK3 were subcloned into a pcDNA3 vector between EcoRI and NotI sites. All restriction enzymes were from New England Biolabs (Ipswich, MA). The final construct consisted of full-length arrestin-3 followed immediately by full-length JNK3 without an additional linker between the coding sequences.

JNK3 phosphorylation assay in HEK293 arrestin-2/3 knockout cells. HEK293 arrestin-2/3 knockout cells (a generous gift from Dr. Asuka Inoue, Graduate School of Pharmaceutical Sciences, Tohoku University) were maintained in DMEM solution containing 10% FBS (Invitrogen), penicillin, and streptomycin at 37°C and 5% CO_2. Cells were transfected at 90-100% confluency in 6-well plates with pcDNA3-HA-ASK1 (0.1ug), pcDNA3-HA-JNK3α2 (0.65µg), and pcDNA3-arrestin constructs (0-0.5µg) at a 1:2.5 ratio of DNA:Lipofectamine 2000 (Invitrogen). At 48 hr post-transfection, the cells were lysed with 400 µL RIPA buffer and spun at 15,000xg to pellet debris. The supernatant was mixed 1:1 with 2x SDS sample buffer (Sigma), the proteins were subjected to 10% SDS-PAGE, and transferred to PVDF membrane (Millipore, Bedford, MA). Membranes were blocked by 1% non-fat dry milk in TBS/Tween-20, incubated with respective primary antibodies (Cell Signaling Technology, Inc.): anti-HA (#3724), anti-phospho-JNK (#9255S), and anti-arrestin (rabbit polyclonal F431 antibody (21)), followed by the appropriate HRP-conjugated secondary antibodies (Jackson ImmunoResearch Laboratories, Inc., West Grove, PA). Bands were detected by X-ray film using enhanced chemiluminescence (ECL, Pierce) and quantification was done using the software Quantity One (BioRad, Hercule, CA).

References

1. Pleinis JM, Davis CW, Cantrell CB, Qiu DY, & Zhan X (2017) Purification, auto-activation and kinetic characterization of apoptosis signal-regulating kinase I. *Protein Expression and Purification* 132:34-43.
2. Vishnivetskiy SA, Zhan X, Chen Q, Iverson TM, & Gurevich VV (2014) Arrestin expression in E. coli and purification. *Curr Protoc Pharmacol* 67:Unit 2.11.11-19.
3. Zhan X, Kaoud TS, Dalby KN, & Gurevich VV (2011) Non-visual arrestins function as simple scaffolds assembling the MKK4–JNK3a2 signaling complex. *Biochemistry* 50(48):10520-10529.
4. Chen Q, *et al.* (2017) Structural basis of arrestin-3 activation and signaling. *Nature Communications* 8(1):1427.
5. Yan C, Kaoud T, Lee S, Dalby KN, & Ren P (2011) Understanding the Specificity of a Docking Interaction between JNK1 and the Scaffolding Protein JIP1. *The Journal of Physical Chemistry B* 115(6):1491-1502.
6. Bartoschik T, *et al.* (2018) Near-native, site-specific and purification-free protein labeling for quantitative protein interaction analysis by MicroScale Thermophoresis. *Scientific Reports* 8(1):4977.
7. Tso S-C, *et al.* (2018) Using two-site binding models to analyze microscale thermophoresis data. *Analytical Biochemistry* 540-541(Supplement C):64-75.
8. Scheuermann TH, Padrick SB, Gardner KH, & Brautigam CA (2016) On the acquisition and analysis of microscale thermophoresis data. *Analytical Biochemistry* 496:79-93.
9. Zhan X, Perez A, Gimenez LE, Vishnivetskiy SA, & Gurevich VV (2014) Arrestin-3 binds the MAP kinase JNK3a2 via multiple sites on both domains. *Cellular signalling* 26(4):766-776.
10. Zhan X, *et al.* (2016) Peptide mini-scaffold facilitates JNK3 activation in cells. *Scientific Reports* 6:21025.
11. Yim YY, Betke K, & Hamm H (2015) Using Peptide Arrays Created by the SPOT Method for Defining Protein-Protein Interactions. *Protein-Protein Interactions: Methods and Applications*, eds Meyerkord CL & Fu H (Springer New York, New York, NY), pp 307-320.
12. Lopez CF, Muhlich JL, Bachman JA, & Sorger PK (2013) Programming biological models in Python using PySB. *Mol Syst Biol* 9:646.
13. Bar-Even A, *et al.* (2011) The moderately efficient enzyme: evolutionary and physicochemical trends shaping enzyme parameters. *Biochemistry* 50(21):4402-4410.
14. Aldridge BB, Burke JM, Lauffenburger DA, & Sorger PK (2006) Physicochemical modelling of cell signalling pathways. *Nature Cell Biology* 8:1195.
15. Zheng L-S, *et al.* (2012) A continuous spectrophotometric assay for mitogen-activated protein kinase kinases. *Analytical Biochemistry* 421(1):191-197.
16. Shockley EM, Vrugt JA, & Lopez CF (2018) PyDREAM: high-dimensional parameter inference for biological models in python. *Bioinformatics* 34(4):695-697.
17. Vrugt JA & C.J.F. tB (2011) DREAM(D): An adaptive Markov chain Monte Carlo simulation algorithm to solve discrete, noncontinuous, and combinatorial posterior parameter estimation problems. *Hydrology and Earth System Sciences* 15(12):3701-3713.
18. Ho DT, Bardwell AJ, Grewal S, Iverson C, & Bardwell L (2006) Interacting JNK-docking sites in MKK7 promote binding and activation of JNK mitogen-activated protein kinases. *J Biol Chem* 281(19):13169-13179.
19. Bai H, *et al.* (2010) Predicting kinetic constants of protein–protein interactions based on structural properties. *Proteins: Structure, Function, and Bioinformatics* 79(3):720-734.
20. Kennedy J & Eberhart R (1995) Particle swarm optimization. *Proceedings of ICNN'95 - International Conference on Neural Networks*, pp 1942-1948 vol.1944.
21. Alvarez-Curto E, *et al.* (2016) Targeted Elimination of G proteins and Arrestins Defines their Specific Contributions to both Intensity and Duration of G protein-Coupled Receptor Signalling. *Journal of Biological Chemistry*.
22. Seo J, Tsakem EL, Breitman M, & Gurevich VV (2011) Identification of Arrestin-3-specific Residues Necessary for JNK3 Kinase Activation. *Journal of Biological Chemistry* 286(32):27894-27901.

Supplementary Figures

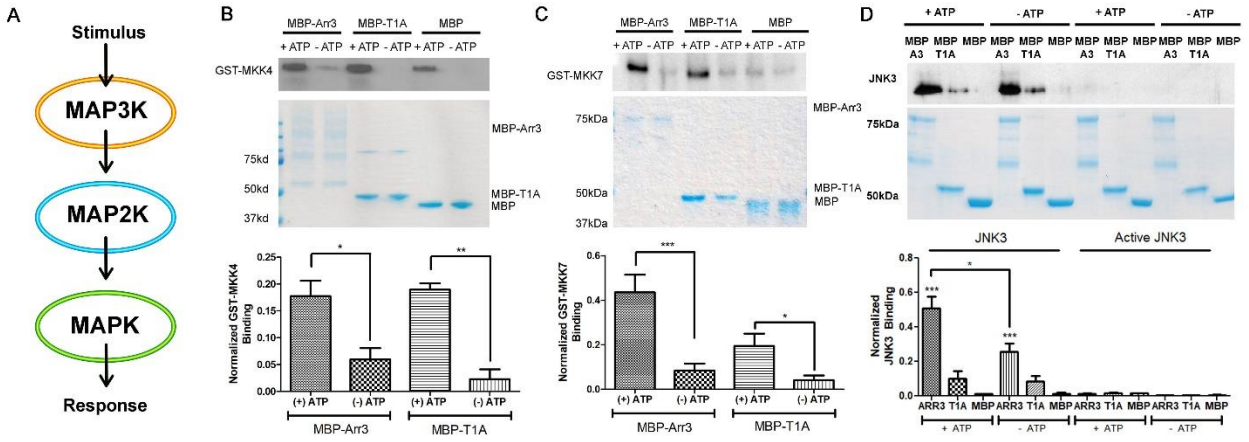

Supplementary Fig. 1. ATP effect on GST-MKK4, GST-MKK7, and His-JNK3 binding to arrestin-3 and T1A peptide. (A) Mitogen-activated protein kinase (MAPK) cascades are three-tiered cascades consisting of a MAP3K, MAP2K, and MAPK. The initial signal or stimulus is propagated through sequential activation (via phosphorylation by an upstream kinase) of each kinase in the cascade. Arrestin-3 acts as a molecular scaffold for these cascades, allowing for signal amplification through production of multiple active MAPKs. **(B-D)** GST-MKK4, GST-MKK7, and His-JNK3 binding to MBP-fusions of arrestin-3 and T1A peptide was determined in the presence and absence of ATP using an in vitro pull-down assay. The upper panel shows a representative Western blot of retained MKK4, MKK7, or inactive and active (doubly-phosphorylated) JNK3, while the lower panel shows a representative Coomassie staining to ensure equal loading of the MBP fusions on the amylose column. Non-specific binding to MBP was subtracted prior to quantitative analysis. Densitometric quantification was performed for each assay using Quantity One software. One-way ANOVA followed by Dunnett's post-hoc test was used to compare the binding in the presence and absence of ATP of each MBP-fusion construct (n=3; *, $p<0.05$; **, $p<0.001$) The student's t-test was used to compare the MBP-arrestin conditions.

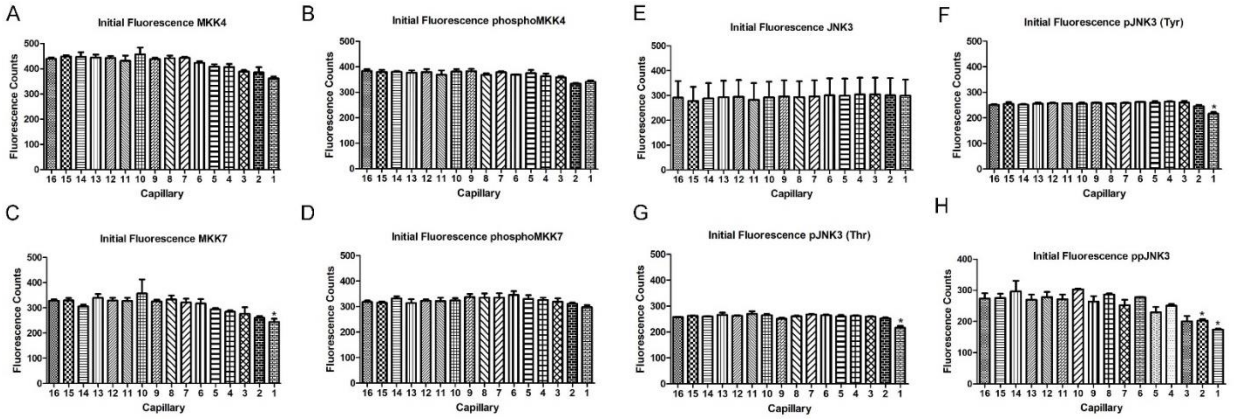

Supplementary Fig. 2. Initial fluorescence of MKK4, MKK7, and JNK3 in the MST assay. Initial fluorescence was measured using a capillary scan prior to MST analysis. Average values of three experiments are shown for unphosphorylated MKK4 **(A),** phosphorylated MKK4 **(B),** unphosphorylated MKK7 **(C),** phosphorylated MKK7 **(D),** unphosphorylated JNK3 **(E),** phosphorylated JNK3 (Tyr) **(F)**, phosphorylated JNK3 (Thr) **(G)**, and doubly phosphorylated JNK3 **(F).** Statistical analysis was performed using NT Analysis Software (NanoTemper technologies GmbH) (*, outside of ±10% interval). An SD Test was performed for data points outside of the 10% interval. It was determined that high concentrations of arrestin-3 yielded ligand-induced fluorescent change. These points were not used in analysis.

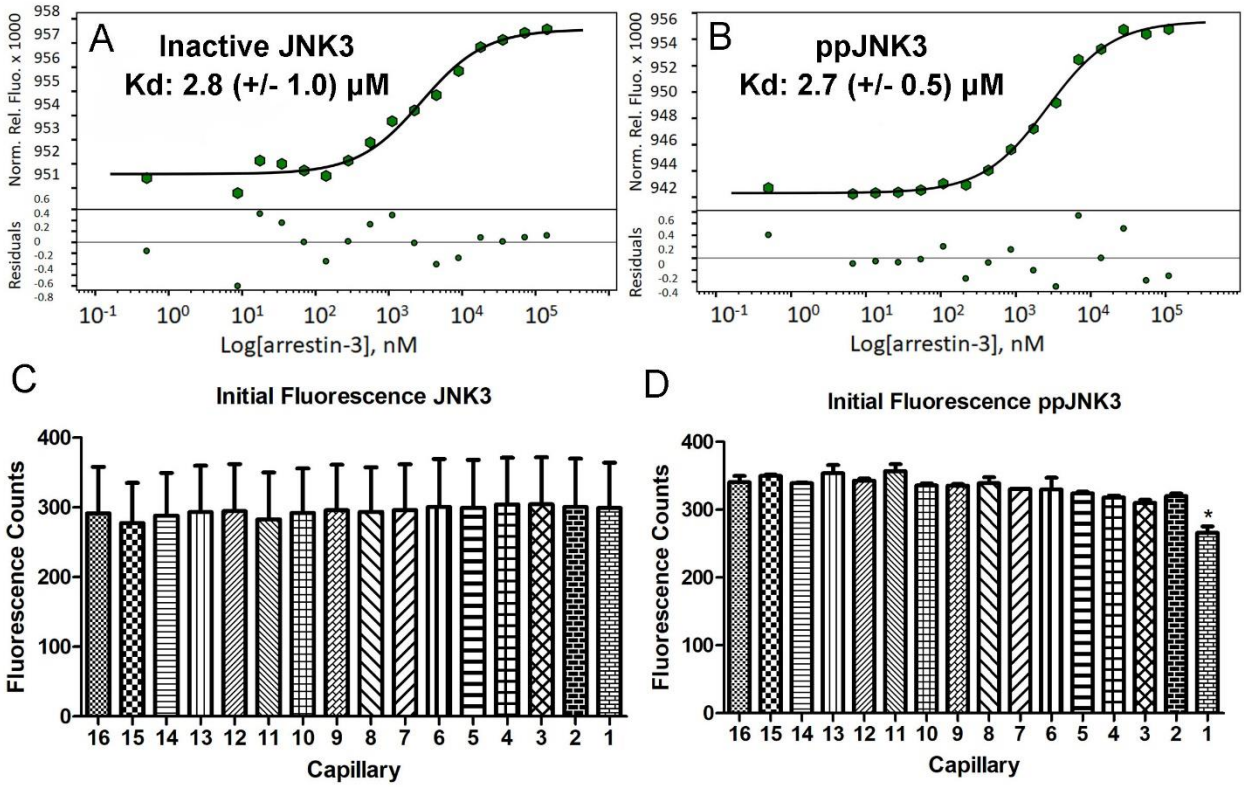

Supplementary Fig. 3. The affinity of arrestin-3 for unphosphorylated and phosphorylated JNK3 measured by MST in the absence of ATP. The K_d values are shown for each curve. **A.** Binding curve for inactive JNK3 and arrestin-3 in the absence of ATP. MST was performed at a constant concentration of Tris-NTA-labeled His-JNK3 (100 nM), and the indicated concentrations of unlabeled arrestin-$3^{(1\text{-}393)}$ (0-72 µM; n=3). **B.** Binding curve for active JNK3 and arrestin-3 in the absence of ATP. MST was performed at a constant concentration of Tris-NTA-labeled His-phosphoJNK3 (100 nM) with a titration with unlabeled arrestin-3 (0-110 µM; n=3). **C,D.** Initial fluorescence was measured using a capillary scan prior to MST analysis. Average values of three experiments are shown for inactive JNK3 **(C),** and doubly phosphorylated JNK3 **(D).** Statistical analysis was performed using NT Analysis Software (NanoTemper technologies GmbH) (*, outside of ±10% interval; these points were excluded from curve analysis). Student's two-tailed t-test was used to assess significance between inactive (unphosphorylated) and active (phosphorylated) JNK3 (** $p<0.01$).

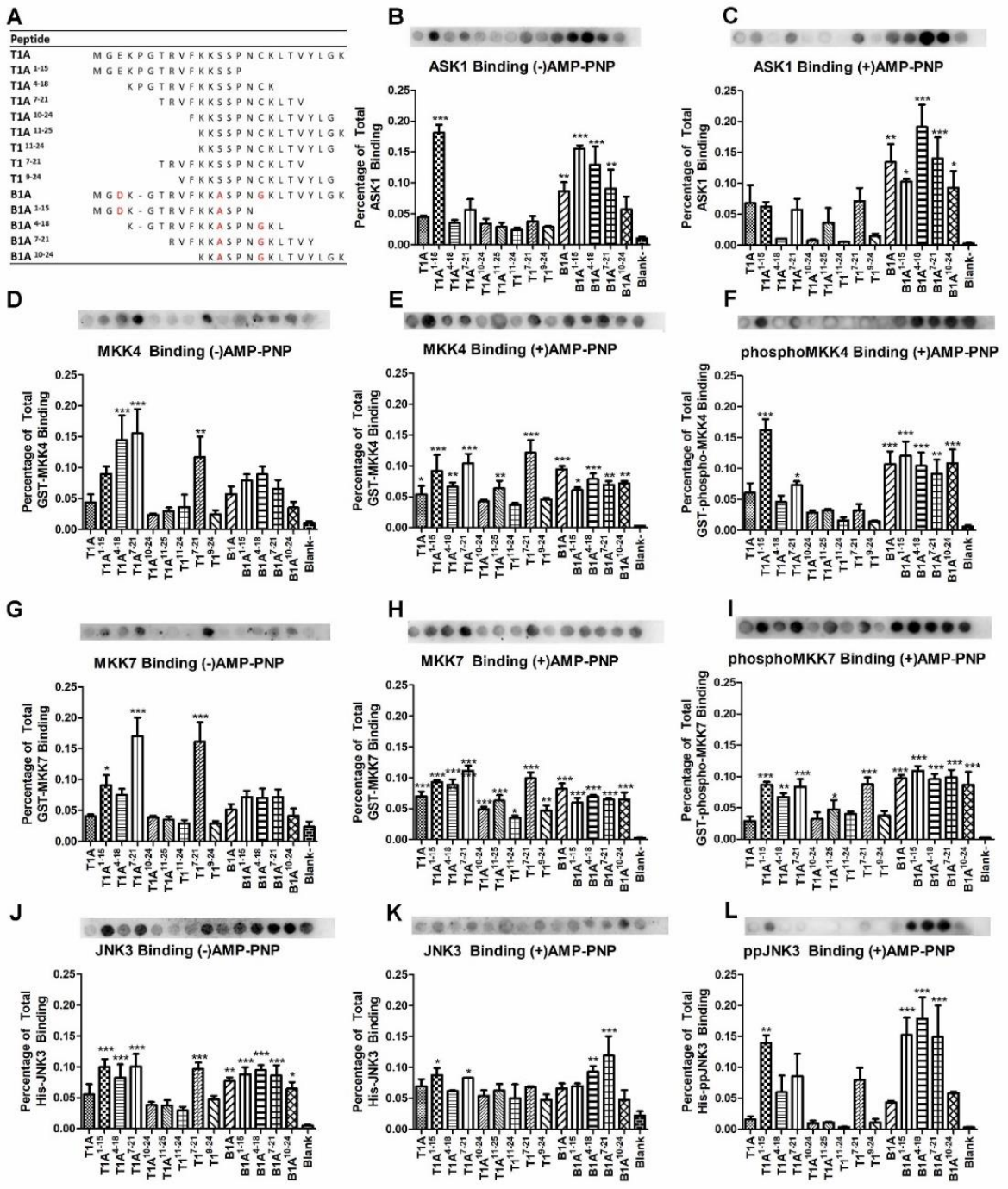

Supplementary Fig. 4. The binding of ASK1, MKK4/7, and JNK3 to arrestin-3 peptides in their unphosphorylated and phosphorylated states. Peptides of the first 25 amino acids of arrestin-3 (T1A) were synthesized as 14-25 amino acid fragments attached to a solid support using ResPep SL (Intavis Bioanalytical Instruments). The amino acid sequences of each peptide and their corresponding names are shown. As a biologically relevant negative control, we added a short scan of the B1A peptide, an N-terminal (homologous to T1A) fragment of arrestin-2, which binds the kinases without facilitating JNK3 activation (22). We also used a blank spot and a 15-mer glycine peptide as negative controls, both of which yielded the same non-specific binding. Sequence differences between the T1A peptide and B1A and B1A-derived peptides are highlighted in red. **B.** The binding of ASK1 in the presence of AMP-PNP, **C.** ASK1 in the absence of AMP-PNP, **D.** GST-MKK4 in the absence of AMP-PNP, **E.** GST-MKK4 in the presence of AMP-PNP, **F.** GST-phosphoMKK4, **G.** GST-MKK7 in the absence of AMP-PNP, **H.** GST-MKK7 in the presence of AMP-PNP, **I.** GST-phosphoMKK7, **J.** JNK3 in the absence of AMP-PNP, **K.** JNK3 in the presence of AMP-PNP, and **L.** phosphoJNK3 (2 mM AMP-PNP and 3 mM $MgCl_2$ when indicated) (n=3-5). Representative peptide array results are shown above graphs displaying experimental averages. Statistical analysis was performed using one-way ANOVA followed by Dunnett's post-hoc test. The statistical significance of the difference of the signal from the blank spot (negative control) is shown (*, $p<0.05$; **, $p<0.01$; ***, $p<0.001$).

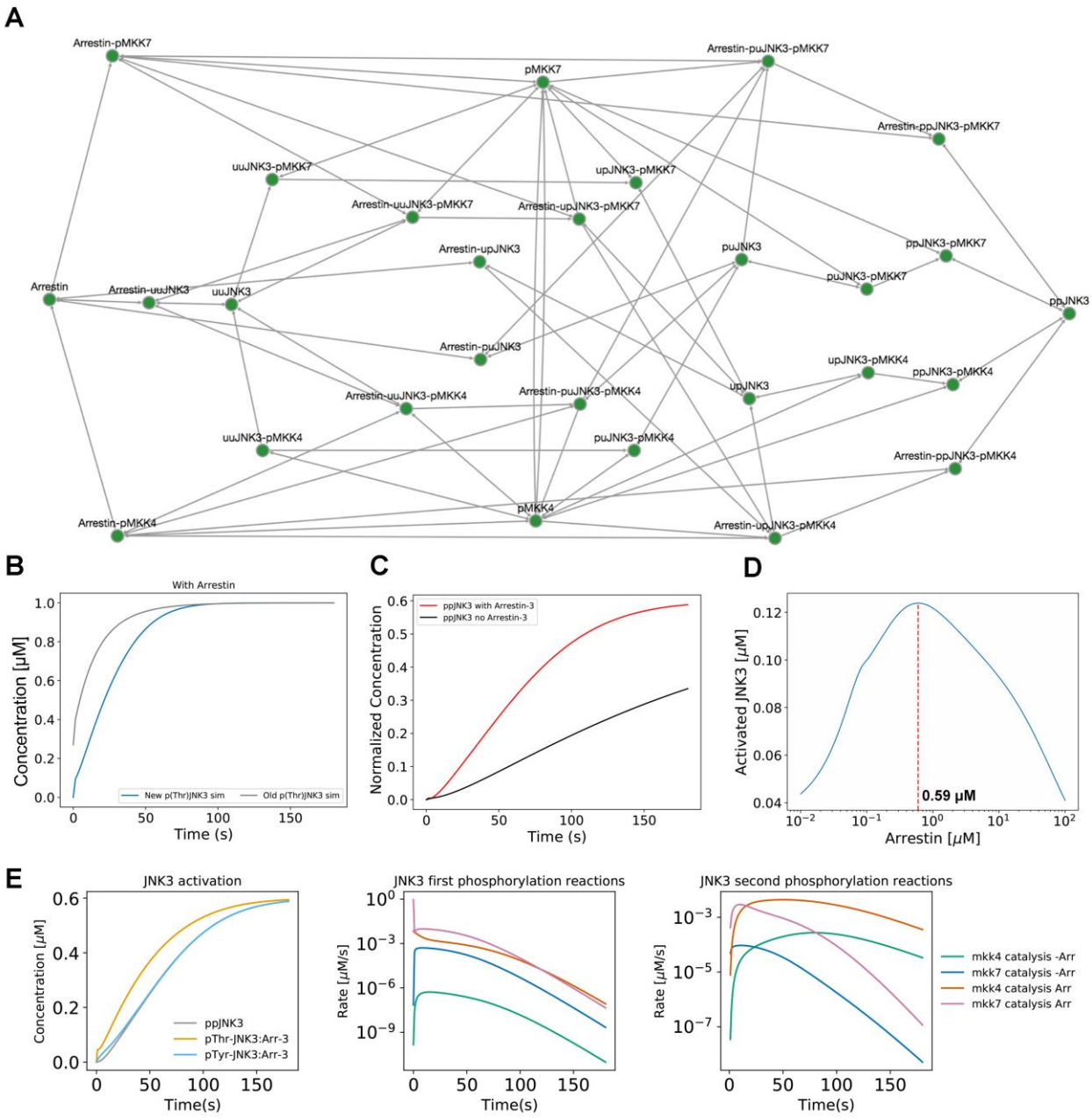

Supplementary Fig. 5. JNK3 activation reaction model. (**A**) The protein-protein interaction networkbetween arrestin-3, MKK4/7 and JNK3. (**B**) Simulated trajectories of Thr-221 phosphorylation in the presence of arrestin-3. As a blind test for JARMv1.0 robustness, the computational model was used to predict phosphorylation of pThr-221 in the presence of data collected using an antibody with limited dynamic range. In this scenario, the experimental results are expected to be inaccurate. The gray line is the proposed trajectory when these inaccurate values for the kinetics of p-Thr221 phosphorylation are used for model calibration and execution. In contrast, the blue line shows the computational model adjusted for the values shown in **Fig. 2B**. This demonstrates that the computational model (gray) accurately predicts the trajectory of the newly collected data (blue) without parameter bias. This validates the model and demonstrates the predicting capabilities of JARMv1.0 for this system in the absence of experimentally determined parameters. **(C)** Simulated model trajectories of doubly phosphorylated JNK3. The red and black lines show the production of ppJNK3 when arrestin-3 is present and absent, respectively. (**D**) Simulated effect of varying arrestin-3 concentration in the system. **(E)** Right panel: corresponds to the time-dependent concentration changes of active (doubly phosphorylated) JNK3, pTyr-JNK3 bound to arrestin-3 and pThr-JNK3 bound to arrestin-3. Center panel: represents the catalysis reaction rate values of singly phosphorylated JNK3. Left panel: shows the catalysis reaction rate values of active (doubly phosphorylated) JNK3.

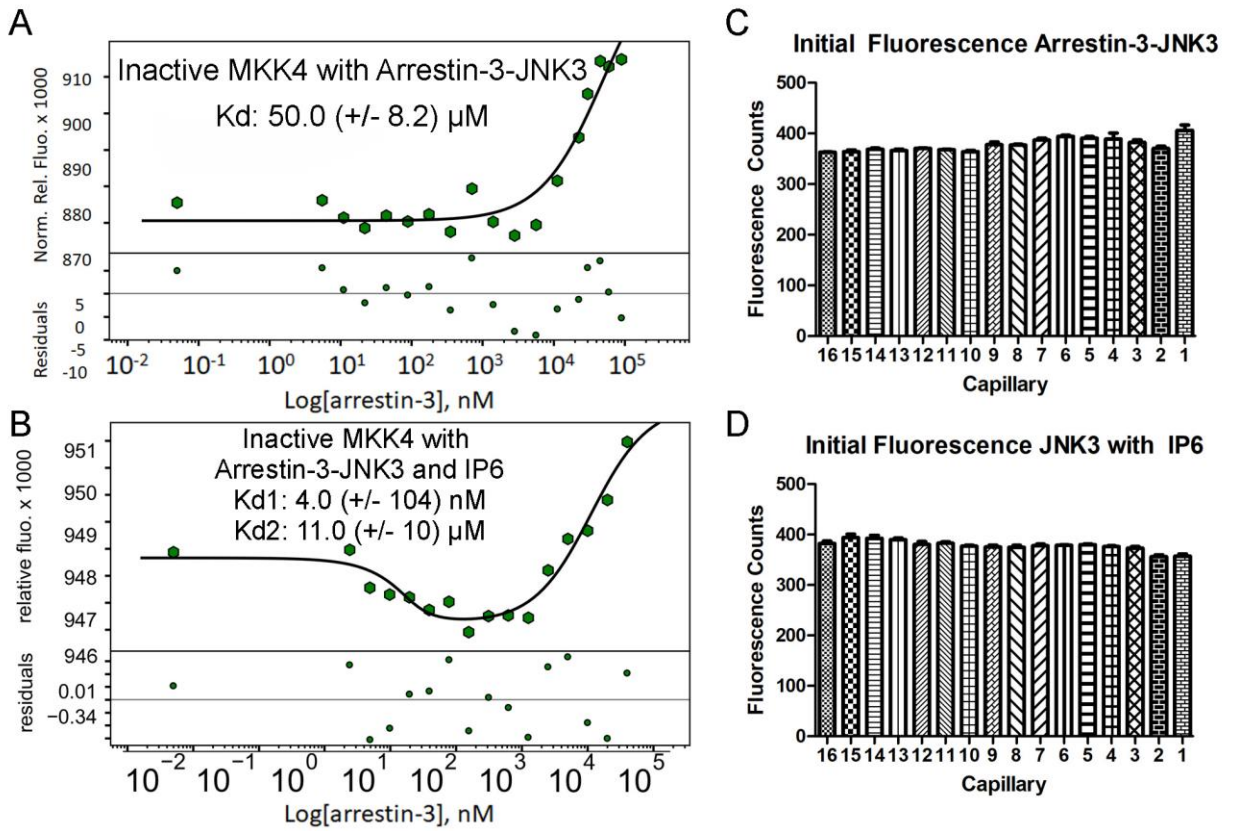

Supplementary Fig. 6. Microscale thermophoresis with an arrestin-3-JNK3 complex or full-length arrestin-3 in the presence of IP_6. The average K_d value is shown. **(A)** The binding curve for arrestin-3-JNK3-His with GST-MKK4 was determined in the presence of 1 mM AMP-PNP and 2 mM $MgCl_2$. MST was performed at a constant concentration of Tris-NTA-labeled arrestin-3-JNK3-His (100 nM), and the indicated concentrations of unlabeled GST-MKK4 (0-90 µM; n=3). Binding curves were calculated using nonlinear regression (curve fit). **(B)** The binding curve for full-length arrestin-3 with inactive JNK3 in the presence of 1 mM AMP-PNP, 2 mM $MgCl_2$, and 100 µM IP_6. MST was performed at a constant concentration of Tris-NTA-labeled His-JNK3 (100 nM) and titrations of full-length arrestin-3 (0-40 µM; n=3). **(C,D)** Initial fluorescence was measured using a capillary scan prior to MST analysis. Average values of three experiments are shown. Statistical analysis was performed using NT Analysis Software (NanoTemper technologies GmbH) (*, outside of ±10% interval; these points were excluded from curve analysis).

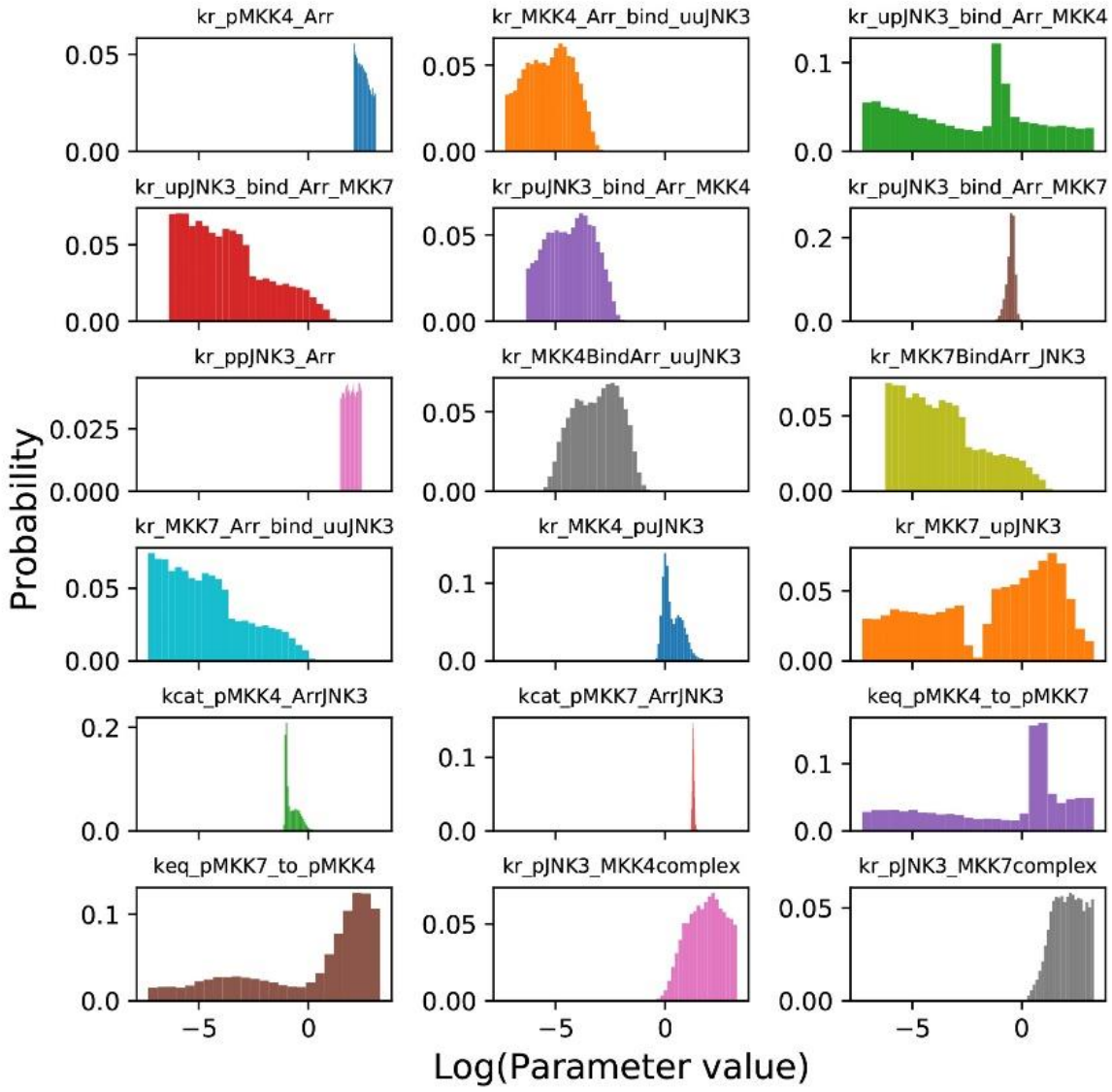

Supplementary Fig. 7. Posterior probability distributions for calibrated JARM kinetic parameters. The x-axis corresponds to the base-10 logarithm range for possible values of kinetic parameters in JARM. The y-axis represents the probability of each of the possible parameter values. The resulting distributions provide an idea of the range and likelihood of each parameter value given the experimental data. As shown, some parameters exhibit a broad range of parameters (~3 orders of magnitude) but the key catalytic parameters for arrestin are well constrained. Parameter values were obtained as described in *SI Methods.* Parameter names with the prefix 'kr', 'kcat' and 'keq' correspond to the reverse, catalysis (sec^{-1} units) and forward ($(uM*sec)^{-1}$ units) rate constants, respectively.